

THE 2023 RELEASE OF CLOUDY

Marios Chatzikos¹, Stefano Bianchi², Francesco Camilloni³, Priyanka Chakraborty⁴,
Chamani M. Gunasekera¹, Francisco Guzmán^{1,5}, Jonathan S. Milby⁶, Arnab Sarkar⁷, Gargi Shaw⁸,
Peter A. M. van Hoof⁹, and Gary J. Ferland¹

Received July 27 2023; accepted August 7 2023

ABSTRACT

We describe the 2023 release of the spectral synthesis code CLOUDY. Since the previous major release, migrations of our online services motivated us to adopt `git` as our version control system. This change alone led us to adopt an annual release scheme, accompanied by a short release paper, the present being the inaugural. Significant changes to our atomic and molecular data have improved the accuracy of CLOUDY predictions: we have upgraded our instance of the Chianti database from version 7 to 10; our H- and He-like collisional rates to improved theoretical values; our molecular data to the most recent LAMDA database, and several chemical reaction rates to their most recent UfA and KiDA values. Finally, we describe our progress on upgrading CLOUDY's capabilities to meet the requirements of the X-ray microcalorimeters aboard the upcoming *XRISM* and *Athena* missions, and outline future developments that will make CLOUDY of use to the X-ray community.

RESUMEN

Se describe el lanzamiento de la versión 2023 del código de síntesis espectral CLOUDY. La migración de nuestros servicios *online* motivó la adopción de `git` como nuevo sistema de control de versiones. Este cambio condujo a un plan de lanzamientos anuales, acompañados de un artículo breve, comenzando por el presente. Cambios significativos en los datos atómicos y moleculares mejoran la exactitud de las predicciones de CLOUDY mediante las actualizaciones de la base de datos de Chianti de la versión 7 a la 10, las transiciones colisionales en iones de uno y dos electrones, los datos moleculares a la versión más reciente de la base de datos LAMBDA y varias constantes de reacción moleculares a los valores de UfA y KiDA más recientes. Finalmente, se describe el proceso de adaptación de CLOUDY a los requisitos de los microcalorímetros a bordo de las misiones *XRISM* y *Athena* y el progreso para hacer CLOUDY útil para la comunidad de astrofísica de rayos X.

Key Words: atomic data — galaxies: active — globular clusters: general — molecular data — software: development

1. INTRODUCTION

CLOUDY is an *ab initio* spectral synthesis code for astrophysical plasmas ranging from far from equilibrium to local thermodynamic equilibrium (LTE) and strict thermodynamic equilibrium (STE). Development started in 1978, and has been ongoing since then, with each new release extending the physical systems the code can model. Previous review papers capture the state of the code at that time, namely, Ferland et al. (1998), Ferland et al. (2013) and Fer-

¹Physics & Astronomy, University of Kentucky, Lexington, Kentucky, USA.

²Dipartimento di Matematica e Fisica, Università degli Studi Roma Tre, via della Vasca Navale 84, 00146 Roma, Italy.

³Max-Planck-Institut für extraterrestrische Physik, Giessenbachstraße, 85748 Garching, Germany.

⁴Center for Astrophysics | Harvard & Smithsonian, Cambridge, MA, USA.

⁵Now at Physics & Astronomy, University of North Georgia, Dahlonega, Georgia, USA.

⁶Arts & Sciences Hive, University of Kentucky, Lexington, Kentucky, USA.

⁷Kavli Institute for Astrophysics and Space Research, Massachusetts Institute of Technology, 70 Vassar St, Cambridge, MA, USA.

⁸Department of Astronomy and Astrophysics, Tata Institute of Fundamental Research, Mumbai 400005, India.

⁹Royal Observatory of Belgium, Ringlaan 3, 1180 Brussels, Belgium.

land et al. (2017). Much of the physics is discussed in Osterbrock & Ferland (2006).

In the past, we aimed to release code only following major changes to the source code and our quantum physics data. The underlying principle had been to deliver our users with a product that would have maximal impact on their research. A consequence of this policy had been infrequent releases, with only seven (7) taking place in the period 1998-2017. The 2006-2010 releases (C06, C07, C08, and C10) were not accompanied by a review paper, which may have left some users wondering how significant the changes in each new version were. Subsequent releases were accompanied by a major review article of CLOUDY's capabilities, which further delayed each release. In this dilemma, we had contemplated if a better release policy might be pursued.

The changes described in § 2 were the impetus we needed to adopt a new release policy. This has essentially been enabled by transitioning to the `git` version control system, which makes branch updates trivial, and eases the process of bringing them back into the mainline of the code. With this in place, we are now able to implement our previous aspirations: annual code releases, each accompanied by a light-weight *release* paper.

The present describes the 2023 release of CLOUDY (C23), a major update to C17 in terms of atomic data, and it is structured as follows. § 2 describes the major changes that the project has undergone these past few years. § 3 and § 4 describe changes to our atomic and molecular data. § 5 outlines recent improvements to our treatment of grains. § 6 presents a summary of improvements to CLOUDY's X-ray capabilities. § 7 and § 8 deal with other improvements and new SEDS in CLOUDY, respectively. § 9 describes changes to CLOUDY infrastructure, including commands. Finally, § 10 discusses current development efforts that should be released in the next few years, as well as our aspirations for future development.

2. ONLINE MIGRATION

Fundamental changes to our infrastructure have occurred in the last few years, most of them happening in Fall of 2019 and Fall of 2020. First, we were forced to move our user forum to a new website. Then, in Fall 2020, our project was forced to vacate the servers that hosted <https://www.nublado.org>, due to policy changes following the acquisition of the host company by a third party. The University of Kentucky has hosted our server since then. The migration to a new server allowed us to migrate to

a more modern control system, as well, namely `git`. As described below, one of us (JM) carried out the Fall 2020 migration.

2.1. Migration of *nublado.org*

There were few (if any) viable options for migrating the entire project to a new host without significant manual intervention. That being the case, it was decided that this was an opportunity to migrate CLOUDY to more modern and flexible version control and tooling. Trac¹⁰ is rather dated at this point. It has not seen a significant update in many years, and it is built on Python 2.x, which is no longer being developed or supported. Subversion¹¹ (SVN) is still actively maintained, but many development projects have moved to using Git, which has a larger community of users and developers. After reviewing options for Git project hosting, it was ultimately decided to use GitLab¹² hosted at UK for the CLOUDY source code, issue tracker, and wiki. GitLab offers a free, open-source edition and provides free access to their licensed features and support services for open-source research software.

Migrating the existing data to GitLab in its entirety would be a difficult task. The existing SVN repository contained several decades of revision history, and the Trac interface held a large number of wiki articles and issue data. It was decided that the existing code revision history would not be migrated to Git. Instead, there would be an initial commit in the Git repository containing a reference to the Subversion repository for historical purposes. This greatly simplified the migration process. Issue data and wiki pages were migrated to GitLab using TracBoat¹³. This tool provided a very basic semi-automated migration but did not preserve all aspects of the content. In particular, wiki links were removed and had to be re-added manually.

The existing Trac site and Subversion repository were migrated to a new system at UK for historical reference purposes. They were configured as read-only, and the default destination for project links is redirected to the GitLab instance. Static files, including data sets, were also migrated and continue to be available and updated as needed.

2.2. User Forum Migration

A forum where CLOUDY users can post questions or report problems has been available since

¹⁰<https://trac.edgewall.org/>

¹¹<https://subversion.apache.org/>

¹²<https://about.gitlab.com/>

¹³<https://github.com/tracboat/tracboat>

June 2005. It had been hosted on `yahoo.com` until Fall 2019, when the company decided to withdraw support for groups. A key requirement for choosing a new host was to preserve the history of questions and answers posted on `yahoo.com`. `groups.io` met our needs, and the forum migrated to `https://cloudyastrophysics.groups.io`.

The new platform has allowed for more versatility. Our new setup now features a `Main` group, which preserves and extends our Q&A service. It also carries an `Announcements` group, where important announcements, e.g., about CLOUDY workshops, are made; a `Code` group, where users can share scripts with other users; and finally a `Results` group, where users can share results obtained using CLOUDY with the broader community. Users are encouraged to subscribe to all these groups.

3. ATOMIC PHYSICS

3.1. Upgrade to Chianti Version 10

CLOUDY has now adopted Chianti version 10.0.1. Previously, the code had been using version 7.1, released in 2013. The difficulty with upgrading earlier has been due to the changes the database format since v7.1. To remedy this, we developed a script to reprocess the version 10 data into the version 7 format. A detailed discussion of the script and changes to spectral line predictions as a result of the new database is presented in Gunasekera et al. (2022a). The reprocessing script has been made open-source and is available at `https://gitlab.nublado.org/arrack`.

Due to the large number of additional atomic levels in version 10, the full reprocessed Chianti database is >15 times the size of version 7. Since many of these levels are above the ionization limit of the corresponding species, we have omitted all auto-ionizing levels from the default version utilized by CLOUDY. Both the full reprocessed v10 database and the one without the auto-ionizing levels can be downloaded from `http://data.nublado.org/chianti/`.

3.2. Updates to the Stout Database

The format of the Stout (Lykins et al. 2015) data files has been updated¹⁴. The most important change is that the spectroscopic information must now be enclosed in double quotes in the `*.nrg` files. This makes it easier for the code to extract this information, which is now included in the `save line labels` output. Also, the keywords in the

`*.coll` files have been updated to make parsing easier. The new format is designated by the magic number “17 09 05”.

The Stout database now supports having multiple atomic or molecular datasets for a given species. This is necessary because it is not always possible to unequivocally decide which calculation is the better one. In such a case, one of these datasets will be designated as the default set, but the user has the option to switch to a different set using the new option to the `species` command. For example, in the command `species “Fe+6” dataset=“alt”`, `alt` is the nickname for the alternate dataset; CLOUDY will use the data in the `Fe_7_alt.*` for this species.

Fe III collision strengths are updated to Badnell & Ballance (2014). We had previously used data from Zhang (1996). Energies are from NIST with missing levels taken from Badnell & Ballance (2014). Laha et al. (2017) describe how the data were matched to experimental energies. Tests show that the total Fe III cooling increases by nearly 50%.

Certain “baseline” models (i.e., models without accurate collisions, see Ferland et al. 2017) in the Stout database have been updated to use collisional, transition probability, and energy data from the ADAS database. NIST energies are employed for the lowest excited levels, to permit the correct identification of spectral lines of astronomical interest. The species that have been updated include Mg^{+9} (Liang & Badnell 2011), Al^{+2} (Liang et al. 2009), and S^{+4} (Fernández-Menchero et al. 2014).

3.3. Fe II

The Fe II ion has a complex structure with 25 electrons, and is a “grand challenge” problem in atomic physics. An accurate set of radiative and collisional atomic data is therefore needed to treat selective excitation, continuum pumping, and fluorescence, which are known to be crucial for the Fe II emission (e.g., Verner et al. 2000; Baldwin et al. 2004; Bruhweiler & Verner 2008; Jin et al. 2012; Wang et al. 2016; Netzer 2020). Uncertainties in the atomic data have been a longstanding limitation in interpreting line intensities.

Until recently, CLOUDY shipped with the Verner et al. (1999) model, which has 371 levels that reach 11.6 eV, has about 68,000 transition probabilities, but uses the “g-bar” approximation for collision strengths. Due to its limitations, Sarkar et al. (2021) explored three other atomic models, that are now available with CLOUDY; their energy levels are compared in Figure 1.

Of relevance to the 2000–3000Å ultraviolet range are the datasets of Tayal & Zatsarinny (2018) and

¹⁴For a full description of the new format see `https://gitlab.nublado.org/cloudy/cloudy/-/wikis/StoutData`.

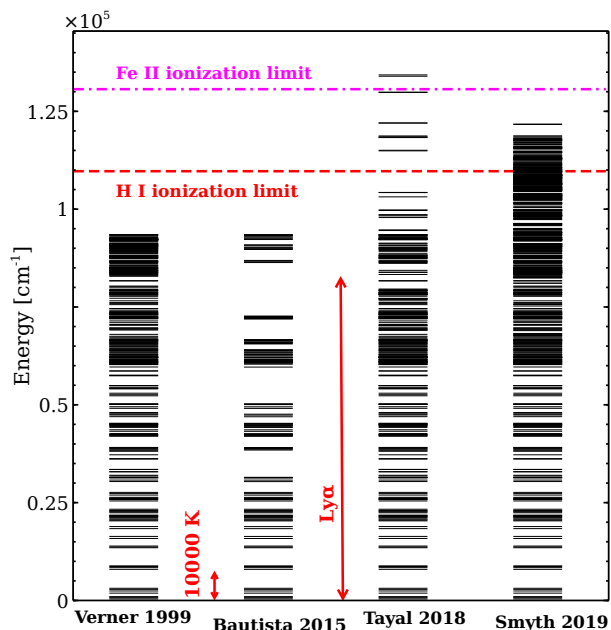


Fig. 1. Energy level structure of the Fe II models available with CLOUDY. From left to right, the atomic datasets are those of Verner et al. (1999), Bautista et al. (2015), Tayal & Zatsarinny (2018), and Smyth et al. (2019). The H I and Fe II ionization limits, the Ly α energy, an important source of photoexcitation for Fe II, and the thermal energy corresponding to 10^4 K are also indicated. Adapted from Sarkar et al. (2021). The color figure can be viewed online.

Smyth et al. (2019). The Tayal & Zatsarinny (2018) model has 340 energy levels with the highest energy of ≈ 16.6 eV, that is, it goes above the ionization limit (16.2 eV). However, its density of states in high-lying energy levels is low, as shown in Figure 1. Transitions between these energy levels produce about 58,000 emission lines with uncertainties in transition probabilities of $\lesssim 30\%$ (in the 2200Å–7800Å). On the other hand, the Smyth et al. (2019) model includes 716 levels in the close coupling (scattering model) calculation, with the highest energy level reaching 26.4 eV. These levels produce about 256,000 emission lines. The Smyth et al. (2019) dataset also contains autoionizing levels, but its density of states in the high-lying energy states is larger than the Tayal & Zatsarinny (2018) dataset. Further details on these atomic models can be found in Sarkar et al. (2021). Both models have been incorporated into CLOUDY.

Sarkar et al. (2021) showed that with the Smyth et al. (2019) dataset, CLOUDY produces a spectrum that is in satisfactory agreement with the template spectrum of the I Zw 1 Seyfert galaxy (Vestergaard & Wilkes 2001). Briefly, the better agreement of the

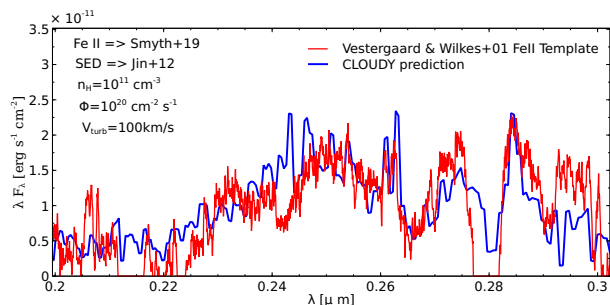


Fig. 2. Comparison between the observed Fe II UV template of Vestergaard & Wilkes (2001) and the CLOUDY predicted Fe II UV spectrum with $V_{\text{turb}} = 100$ km/s. The color figure can be viewed online.

Smyth dataset is due to the higher density of highly excited states, which enhance the effects of continuum fluorescence and lead to brighter emission lines at short wavelengths. Further details are described in the paper. Figure 2 illustrates the quality of that comparison.

3.4. $K\alpha$ Energies

We incorporated precise H-like $K\alpha$ energies for elements between $6 \leq Z \leq 30$ to match laboratory energies (Chakraborty et al. 2020a). Figure 3 compares the difference in $K\alpha$ energies between NIST (Kramida et al. 2018) and CLOUDY for the updated CLOUDY energies and the old CLOUDY energies appearing in C17.02. The revised $K\alpha$ energies are ≈ 15 -4000 times more precise than those of C17.02. This energy precision is also much superior to the energy accuracy of the current and future X-ray instruments like *Chandra*, *XMM-Newton*, *XRISM*, and *Athena*, as shown in Figure 3. The improved CLOUDY energies will therefore be in excellent agreement with the future microcalorimeter observations.

3.5. Inner Shell Energies

We updated the fluorescence $K\alpha$ energies of Si II-XI and S II-XIII used in CLOUDY with the experimental data reported in Hell et al. (2016). The energies of the lines in the past versions of CLOUDY are mainly taken from Table 3 of Kaastra & Mewe (1993), which contains the fluorescence yields, energies and Auger electron numbers for elements and ions from Be to Zn. Even though these values were in accordance with the theoretical calculations available at the time of the publication, today, this dataset is not accurate enough to model some already available high-resolution spectra (Amato et al. 2021; Camilloni et al. 2021), and certainly for future X-ray spectra having eV resolution.

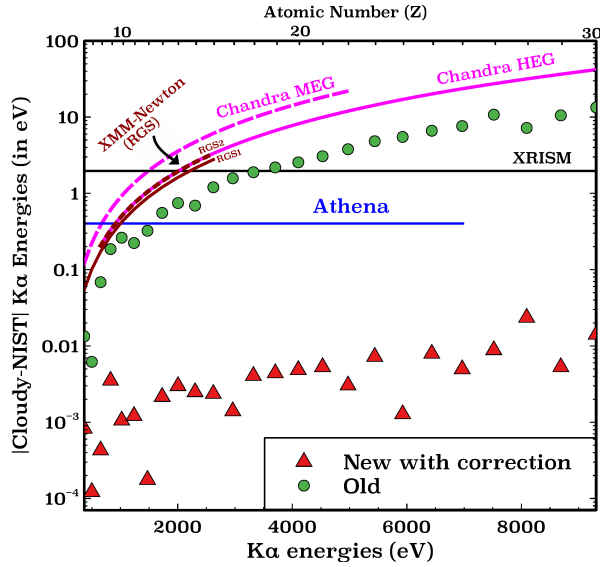


Fig. 3. The absolute value of the difference between NIST and CLOUDY $K\alpha$ energies versus $K\alpha$ energies for H-like ions of elements between $6 \leq Z \leq 30$. Red triangles show the difference between energies in the current version (as of C17.03) of CLOUDY and NIST, while green circles show the same difference for previous versions of CLOUDY (from ≈ 2005 to C17.02). The color figure can be viewed online.

For this reason, we updated the energies from O-like to Be-like ions of Si and S (Si VII-XI and S IX-XIII) adopting the centroids for unresolved blends given in Table 3 of Hell et al. (2016). Regarding the low-ionization lines, individual energies are taken from their Table 5, where the values of Si II-IV, Si V-VI, S II-VI and S VII-VIII are listed. $K\alpha_1$ and $K\alpha_2$ are not experimentally resolved in Hell et al. (2016), and their difference in energy is lower than the expected resolution of future X-ray microcalorimeters, so we assumed the same energy for both. Camilloni et al. (2021) provided a demonstration of the impact that such an update can have on the high-resolution spectra of the high mass X-ray binary Vela X-1 (see Figure 4).

3.6. ℓ -changing Collisions

Momentum-changing collisions by protons were deeply revised in C17. An upgrade of the theory of Pengelly & Seaton (1964, hereafter PS64), dubbed PS-M, was published by Guzmán et al. (2017b), correcting the results at high density and low temperature of PS64 and getting a better agreement with the quantum-mechanical *ab initio* results from Vrinceanu & Flannery (2001, hereafter VF01). The theory has been further refined by Badnell et al. (2021), now called PS-M20. PS-M/PS-M20

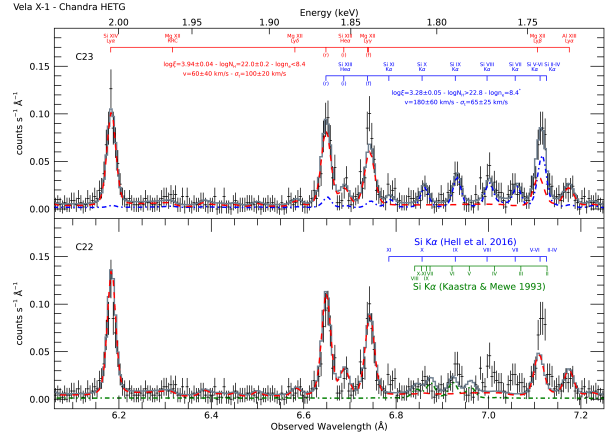


Fig. 4. Visually co-added *Chandra* MEG ± 1 order spectra of the HMXB Vela X-1 at the orbital phase $\phi_{orb} = 0.75$ (see Amato et al. 2021). *Top*: Best fit model with CLOUDY (grey solid line), using the improved energies for the Si fluorescence lines, available in C23. The specific contributions of each gas component are labeled (red dashed line and blue dot-dashed line), together with the best-fit parameters and 90% confidence level uncertainties (see Camilloni et al. 2021, for details). *Bottom*: As above, but with the previous version of CLOUDY, C17. The low ionization component is here labeled in green, together with the adopted Si $K\alpha$ lines (from Kaastra & Mewe 1993). For ease of comparison, the improved energies from Hell et al. (2016) are in blue, as in the top panel. Adapted from Camilloni et al. (2021). The color figure can be viewed online.

results were in better agreement with the quantal calculations than the semi-classical calculations from Vrinceanu et al. (2012) (hereafter VOS12), which underestimate VF01 by a factor ≈ 6 (Guzmán et al. 2016). Semi-classical rates were corrected by Vrinceanu et al. (2017) to get agreement with VF01 and PS-M. Vrinceanu et al. (2019) report in their Figure 2 a disagreement of PS-M rates with quantum mechanical rates for high n . However, we have confirmed that PS-M rates actually agree with the quantum mechanical ones for the results plotted in their figure. Their reported disagreement can be explained because they calculated the excitation $\ell \rightarrow \ell + 1$ collisions incorrectly using the formula given by Guzmán et al. (2017b), optimized for de-excitation collisions ($\ell \rightarrow \ell - 1$). If micro-reversibility is applied to the results of Vrinceanu et al. (2019) the obtained rates agree with the quantum ones for the entire range of the figure (Badnell et al. 2021).

Guzmán et al. (2017a) compared in their Tables 1 and 2 PS-M effective recombination rates to $n = 2$ levels of hydrogen with the ones quoted in Ta-

bles 4.10 and 4.11 of Osterbrock & Ferland (2006), obtained from Pengelly & Seaton (1964). PS-M produces effective recombination coefficients to $2s$ that are bigger in a $\approx 0.6\%$ for Case A and a $\approx 0.1\%$ for Case B, while recombination to $2p$ is smaller by $\approx 1 - 2\%$. Similarly, they found an agreement up to $\approx 5\%$ for the emissivities of $2s^2S \rightarrow 2p^2P_{3/2}^o$ and up to a $\approx 0.5\%$ for $2s^2S \rightarrow 2p^2P_{3/2}^o \rightarrow 2p^2P_{1/2}^o$. We do not expect this to influence $\text{Ly}\alpha$ or the two-photon emission spectrum.

PS-M20 theory has been implemented in the latest versions of CLOUDY for H-like and He-like ions. CLOUDY selects PS-M20 theory by default if not specified. The command that selects the new PS-M20 results is:

```
database H-like collisions l-mixing
                                Pengelly PSM20
```

for H-like collisions, and

```
database He-like collisions l-mixing PSM20
```

for He-like systems.

3.6.1. The Importance of a Correct Number of Resolved Levels: Printing ℓ -changing Critical Densities

Accurate modeling of recombination lines for H-like and He-like ions requires a good description of the ion energy levels. CLOUDY distinguishes between angular momentum ℓ -resolved levels and *collapsed* levels, for which ℓ -levels are populated according to their statistical weight (see Ferland et al. 2013, for more details).

Critical densities are defined as the density where collisional rates equal radiative de-excitation, $n_{e,c} q_{lu} = \tau_{ul}^{-1}$ (Pengelly & Seaton 1964), where τ_{ul} is the half-life of radiative de-excitation between u and ℓ sub-shells, and q_{lu} is the effective coefficient of collisional excitation between ℓ and u sub-shells. Then averaging over ℓ we can obtain the critical density for the shell n :

$$n_{e,c} = \frac{1}{q_n \tau_n}, \quad (1)$$

for densities above $n_{e,c}$, collisions will be faster than radiative decay and dominate, ultimately bringing the n -shell to be statistically populated in its ℓ -sub-shells.

CLOUDY now has a new command,

```
print critical densities
```

that can be used to print ℓ -changing critical densities for H-like and He-like ions in the output file. This

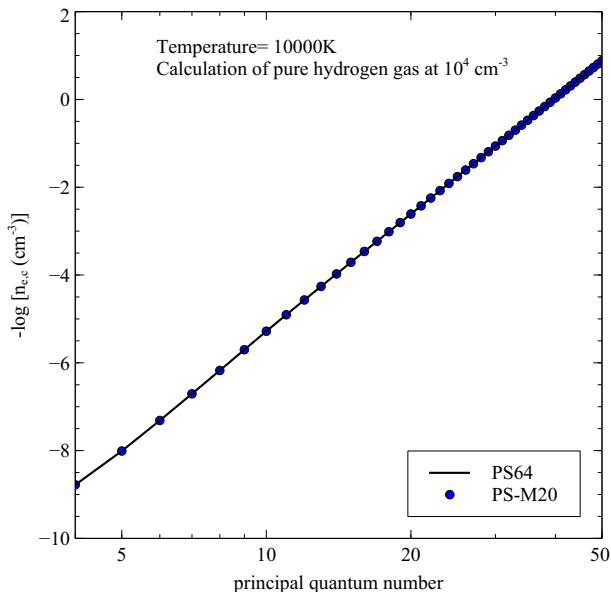


Fig. 5. Comparison of critical densities from equation 1 with ℓ -changing collisions from PS-M20 with the results of Figure 4 of Pengelly & Seaton (1964). We have chosen a pure hydrogen gas at electron temperature $T = 10000\text{K}$ and electron density $n_e = 10^4 \text{cm}^{-3}$. The agreement is complete. The color figure can be viewed online.

command aims to help choose a physically-motivated number of resolved levels to employ in a simulation for each ion.

Optionally, H-like or He-like can be added together with an element name to specifically print the critical densities for an ion. For example, while the command line above prints critical densities for all resolved levels included in the simulations for all H-like and He-like ions, the more specific command,

```
print critical densities H-like
```

prints only critical densities for H-like ions, while

```
print critical densities H-like helium
```

prints only critical densities for the He^+ ion.

In Figure 5 we have plotted the critical densities obtained with CLOUDY using PS-M ℓ -changing theory versus the principal quantum number. Critical densities from Figure 4 of Pengelly & Seaton (1964) are also plotted for comparison. Complete agreement is shown in the figure. When densities are higher than the critical densities, collisions dominate and the ℓ quantum numbers redistribution is faster. At much higher densities the population of the ℓ -sub-shells will be statistical. Figure 5 can be used to determine the number of levels that should be treated as resolved in ℓ . As a rule of thumb, it

is safe to add ten units to the principal quantum number for which the density is critical to ensure that collisions will statistically populate the levels treated as collapsed. For example, in a simulation of an H II region with density $n_e = 10^4 \text{ cm}^{-3}$, the principal quantum number corresponding to that density would be $n \approx 15$, according to Figure 5 (we can use the `print critical density` command to verify the critical densities for all resolved levels). A safe number of resolved levels to use is all levels $n \leq 25$, that can be included in the simulations with the line (Ferland et al. 2017):

```
database H-like hydrogen levels resolved 25
```

Note that different conditions of electron temperature and densities might cause the critical densities to vary, obeying the temperature dependence of the ℓ -changing cross sections, as well as their dependence on density due to the Debye cut-off of the collision probabilities (Pengelly & Seaton 1964; Guzmán et al. 2016).

3.7. *n*-changing Collisions

Principal quantum number-changing electron collision data were analyzed by Guzmán et al. (2019). C17 and previous versions used semi-empirical data from Vriens & Smeets (1980, hereafter VS80). Guzmán et al. (2019) suggested using the semiclassical straight trajectory Born approximation of Lebedev & Beigman (1998, hereafter LB98). The latter is within a factor of ≈ 2 of VS80 collisions and has the same dependency on the high- and low-energy range. Care must be taken when dealing with highly charged ions as the straight trajectory approximation would fail, especially at low energies, producing an underestimation of the rates. In that case, it would not be safer to use VS80, as this is intended only for atoms. Further theoretical work is needed for a better theory for highly charged ions.

While LB98 is the default theory for both H-like and He-like *n*-changing collisions, it is possible to choose between different theories in CLOUDY using the command:

```
database H-like collisions Lebedev
```

where H-like can be modified to He-like and the options are:

- **Lebedev** (default) for semiclassical straight trajectory theory (Lebedev & Beigman 1998).
- **Vriens** for Vriens & Smeets (1980) semi-empirical approximation.

- **Fujimoto** for the semi-empirical formula fit of Fujimoto (1978).
- **van regemorter** for the averaged gaunt factor formula proposed by van Regemorter (1962).

A comparison and analysis of these theories and application to different cases can be found at Guzmán et al. (2019).

3.7.1. *Masing of Hnα Lines*

In contrast to C17, masing of hydrogen lines is now allowed. Guzmán et al. (2019) predict masing of $Hn\alpha$ radio recombination lines for low-density clouds ($n_e \leq 10^8 \text{ cm}^{-3}$). These authors also predict masing of the $Hn\alpha$ lines, with n ranging between 50 and 190, for a model of the Orion Blister. However, the number of masing lines decreases for data sets other than LB98. In these cases, the higher collisional rates bring the populations of the Rydberg levels closer to LTE, thus suppressing masing.

4. MOLECULAR DATA

4.1. H₂

A large model of molecular hydrogen was introduced by Shaw et al. (2005). The level energies, which we use to derive line wavelengths, have been updated to Komasa et al. (2011). This work incorporates many high-order effects in the H₂ wavefunctions, which result in ≈ 1 wavenumber changes in level energies. We derive line wavelengths from these energies, so small changes in wavelength result. The Komasa et al. (2011) energies are thought to be a significant improvement over previous data sets.

The previous version of CLOUDY included the Lique (2015) H – H₂ collisional data as an option, although they were not used by default. We now use this as our preferred H – H₂ collision data set. Compared with previous calculations, these data extend to higher vibrational manifolds and include ortho-para changing reactive collisions. Tests show that the H₂ 2.121 μm line intensity changes by roughly 50%, becoming stronger in some PDR sims.

4.2. *Other Molecules*

Molecular lines are sensitive to underlying physical conditions. Hence, they reveal physical conditions in various astrophysical environments when interpreted correctly. It is always our aim to predict more molecular lines with better precision. We do it in two ways. Firstly, by including more molecules in the CLOUDY molecular network. Secondly, by updating the existing molecular network. Below, we mention such recent efforts.

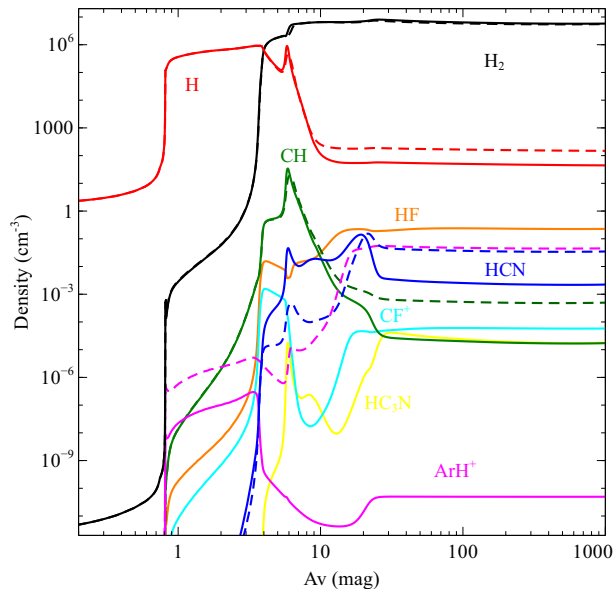


Fig. 6. Variation of densities of a few molecules as a function of A_V for an H II and PDR model (“h2_orion_hii_pdr.in” from the CLOUDY download under the directory `tsuite`). The name of each molecule and the line representing its density are depicted in the same color. The solid lines represent simulations using this version, and the dashed lines represent simulations using an earlier version C17. The color figure can be viewed online.

Shaw et al. (2022) have included the gas-phase energy levels, radiative and collisional rates for HF, CF^+ , HC_3N , ArH^+ , HCl, HCN, CN, CH, and CH_2 into CLOUDY’s molecular network. The energy levels and collisional rate coefficients were taken from the upgraded LAMDA Database (van der Tak et al. 2020). However, reaction rates stem from the UMIST Database for Astrochemistry (UDfA 2012; RATE12), specifically, Roueff et al. (2014); Schilke et al. (2014); Priestley et al. (2017). As a result, CLOUDY now predicts the line intensities and column densities of these molecules in addition to those included in the previous version. Figure 6 (Shaw et al. 2022) shows the variation of densities of a few molecules as a function of A_V . The name of each molecule and the line representing its density are depicted in the same color. The solid lines represent simulations using this version, and the dashed lines represent simulations using the earlier version C17.

Likewise, we have included the gas-phase chemical reactions, energy levels, and radiative and collisional rates of the SiS molecule (Shaw et al. 2023a). The energy levels, Einstein’s radiation coefficients and collisional rate coefficients with H_2 molecules

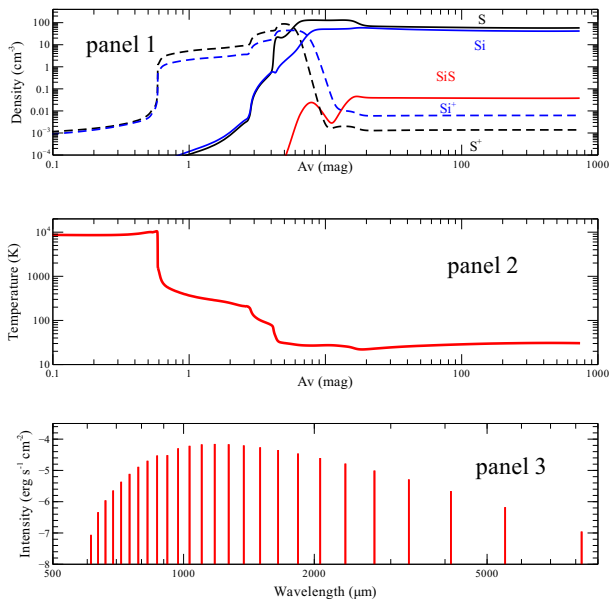


Fig. 7. Panel 1: Variation of SiS density as a function of A_V for an H II and PDR model (“h2_orion_hii_pdr.in” from the CLOUDY download under the directory `tsuite`). Panel 2: Variation of temperature across the cloud. Panel 3: Model predicted intensities of various SiS rotational lines. The color figure can be viewed online.

were taken from the upgraded LAMDA database. In addition, we have included collisions with H (Anusuri 2019) and He (Vincent et al. 2007; Toboła et al. 2008). The chemical reaction rates were taken from various sources, UDfA, namely Zanchet et al. (2018), Willacy & Cherchneff (1998), Doddipatla et al. (2021); and the Kinetic Database for Astrochemistry,¹⁵ respectively. Figure 7 (Shaw et al. 2023a) demonstrates predicted intensities of various rotational lines of SiS for an H II and PDR model (“h2_orion_hii_pdr.in”) from the CLOUDY download under the directory `tsuite`.

Shaw et al. (2023a) included only rotational levels of SiS. However, we have now included the vib-rotational levels (private communication with Ziwei Zhang).

Any species’ predicted column densities and line intensities depend on rate coefficients. We use mostly UDfA rate coefficients. In the UDfA, a two-body gas-phase chemical reaction rate coefficient k ($\text{cm}^3 \text{s}^{-1}$) is given by the usual Arrhenius-type formula,

$$k = \alpha \left(\frac{T}{300} \right)^\beta \exp(-\gamma/T), \quad (2)$$

¹⁵<https://kida.astrochem-tools.org/>

where T is the gas temperature. Reactions with $\gamma < 0$ will become unphysically large at low temperatures. Röllig (2011) has addressed the divergence of rate coefficients at low temperatures. A similar problem occurs for high temperatures encountered with CLOUDY. We apply a temperature cap T_{cap} for $\beta > 0$ to avoid this. For $T > T_{cap}$, the rate coefficients retain the same values as at T_{cap} . Though ad hoc, we choose $T_{cap} = 2500\text{K}$ (Shaw et al. 2023b). This affects the warm, 5000K - 10000K, collisionally ionized clouds.

Cosmic-ray ionization rate plays an important role in ISM and is an active field of research. Shaw & Ferland (2021) demonstrated that the abundance of PAHs affects the free electron density, which changes the H_3^+ density and hence the derived cosmic-ray ionization rate of hydrogen. We suggested that for the average Galactic PAH abundance, the cosmic-ray ionization rate of atomic hydrogen be $3.9 \pm 1.9 \times 10^{-16} \text{ s}^{-1}$. The command

```
cosmic rays background 1.95 linear
```

sets this rate. Furthermore, we showed that the cosmic-ray ionization rate of hydrogen derived using H_3^+ is much higher when PAHs are absent.

Furthermore, Shaw et al. (2020) updated the mean kinetic energy of the secondary electrons (from 20 eV to 36 eV) produced by cosmic rays. This affects the cosmic-ray dissociation of molecular hydrogen and dense cloud chemistry.

5. GRAIN DATA

5.1. *New Refractive Index Files*

New refractive index files have been added for astronomical silicate and graphite using the data described in Draine (2003). These add much more structure to the inner-shell photoionization edges seen in the X-ray regime.

5.2. *Interstellar Grain Absorption*

We have introduced a new option to the `metals deplete` command to use the more self-consistent depletion pattern described in Jenkins (2009). An in-depth discussion on this depletion pattern and how it affects the predicted spectra is presented in Gunasekera et al. (2022b, 2023). This new element-selective depletion option can be enabled with the

```
metals deplete Jenkins 2009
```

command. The depletion parameters A_X , B_X , and z_X , specific for each element X , are read in from

an external file called `Jenkins09_ISM.Tab4.dep`, and are used to compute the depletion scale factor D_x using the equation

$$D_x = 10^{B_X + A_X(F_* - z_X)}, \quad (3)$$

where F_* represents the degree of depletion across all elements. This D_x factor then multiplies the reference abundance to produce the post-depletion gas-phase abundances. By default, $F_* = 0.5$. However, its value may be adjusted with the command

```
metals depletion jenkins 2009 fstar <value>
```

where the `<value>` must range between 0 and 1.

An analysis of strong spectral-lines ($\log([\text{O III}] \lambda 5007/\text{H}\beta)$, $\log([\text{N II}] \lambda 6583/\text{H}\alpha)$, $\log([\text{S II}] \lambda \lambda 6716, 6731/\text{H}\alpha)$, and $\log([\text{O I}] \lambda 6300/\text{H}\alpha)$) from a CLOUDY model of a generalized H II region, based on SDSS-IV MaNGA observations (Bundy et al. 2015; Yan et al. 2016), revealed that varying F_* affects the spectral line intensities and the thermal balance of the ionized cloud (Gunasekera et al. 2023). The user must alter the grain abundance to match the degree of depletion (F_*). To do this, compute the fraction of the total abundance of heavy elements locked in dust grains in the given F_* relative to the total abundance of heavy elements locked in dust grains at $F_* = 0.5$,

$$grains = \frac{\sum_X (X_{dust}/H)_{F_*}}{\sum_X (X_{dust}/H)_{0.5}}. \quad (4)$$

This fraction can then be given in the `grains` command to change the dust abundance self-consistently.

6. X-RAY PREDICTIONS

6.1. *Microcalorimeters*

Historically, CLOUDY made X-ray predictions but was not designed for high-resolution spectral analysis. In preparation for the upcoming microcalorimeter missions *XRISM* and *Athena*, we have extended CLOUDY to make it compatible with high-resolution spectral analysis in the X-ray regime. Chakraborty et al. (2020b) demonstrated the effects of Li-like iron on the Fe XXV $K\alpha$ line intensities via resonant Auger destruction (RAD; e.g., Ross et al. 1978; Matt et al. 1996; Liedahl 2005). Although initially motivated by the Perseus cluster, this analysis was extended to include a wide range of column densities encountered in astronomy.

We also showed line-broadening effects produced by electron scattering. The command `no scattering escape` was introduced to ignore

scattering of photons off of thermal electrons (Chakraborty et al. 2020b). When line photons scatter off high-speed electrons, a fraction of them receive large Doppler shifts from their line center, creating super-broad Gaussian profiles. Such broad line profiles will not be detected in future high-resolution X-ray telescopes. The purpose of the above command is to model the unscattered photons that will be observed by these future X-ray missions. The command `no absorption escape` was introduced to ignore absorption by background opacities.

Comparing the observed spectra by *Hitomi* with CLOUDY simulated spectra, Chakraborty et al. (2020c) presented a novel diagnostic for measuring column densities transitioning from optically thin (Case A) to optically thick (Case B) in H- and He-like iron. The effects of metallicity and turbulence on Fe XXV $K\alpha$ line ratios were also demonstrated using the Perseus cluster as a reference.

We have also updated the collision strengths of the Fe $K\alpha$ lines using recent calculations by Si et al. (2017), replacing the old collision rates by Zhang & Sampson (1987). The new rates are calculated based on the independent process and isolated resonance approximation using distorted waves (IPIRDW) technique. Updates to the collision rates resulted in significant differences in the estimated Fe $K\alpha$ line ratios, as described in Chakraborty et al. (2020c).

Chakraborty et al. (2021) extended the classic Case A and Case B (Osterbrock & Ferland 2006) to less familiar regimes Case C and Case D in the X-ray band. Previous works on these limits focused on the optical, ultraviolet, and infrared regimes (Menzel 1937; Baker & Menzel 1938; Chamberlain 1953; Ferland 1999; Peimbert et al. 2017), but X-ray wavelengths were rarely studied. The net X-ray spectrum for all four cases within the energy range 0.1-10 keV was simulated at the resolving power of *XRISM*.

Chakraborty et al. (2022) demonstrated atomic processes modifying soft X-ray spectra. This includes the enhancement in line intensities via continuum pumping in photoionized environments, and suppression in line intensities through photoelectric absorption and electron scattering in collisionally-ionized and photoionized environments. A hybrid of CLOUDY simulated collisionally-ionized and photoionized model was used to fit the *Chandra* Medium Energy Grating (MEG) spectrum from V1223 Sgr, an intermediate polar. This was the first application of the new CLOUDY interface compatible with high-resolution spectral analysis in the X-ray regime.

We also increased the default number of levels in our default instance of the Fe¹⁶⁺ ion. The default limit to the number of its levels suppressed the 15.013 Å line, which is prominent in soft X-ray spectra. Ferland et al. (2017) has an extensive discussion of our choice of a default number of levels, the effects on a calculation, and how to change it.

Finally, we have improved the energy grid resolution of CLOUDY's coarse continuum to better suit it for tailoring models to the upcoming *XRISM* mission.

6.2. Inner Shell Ionization

The X-ray portion of most SEDs has little effect on the ionization of an ionized cloud, as discussed for AGN in the first appendix of Temple et al. (2023). A more general discussion is presented here.

The photoionization rate for a given shell n is

$$\Gamma_n = \int_{\nu_0}^{\infty} \sigma_\nu \phi_\nu d\nu \quad [\text{s}^{-1}], \quad (5)$$

where ν_0 , σ_ν are the photoionization threshold of shell n [Ryd] and the cross section [cm^{-2}], respectively, and ϕ_ν is the flux of ionizing photons [$\text{cm}^{-2} \text{s}^{-1} \text{Ryd}^{-1}$]. The total photoionization rate is the sum over all shells is

$$\Gamma_{total} = \sum_n \Gamma_n \quad [\text{s}^{-1}]. \quad (6)$$

Consider the case of O²⁺, a common ion of the 3rd most abundance element which produces the very strong O III lines. Three subshells, $1s^2$, $2s^2$, and $2p^2$, contribute to the total photoionization rate. We use the data fitted by (Verner et al. 1996). The cross sections are shown in Figure 8. The K-shell cross sections are nearly one dex smaller than the valence shell.

The radiation field shape enters in equation 5. Figure 9 shows a power-law continuum, one with $f_\nu \propto \nu^{-1}$. This is an exceptionally hard SED with a large number of K-shell photons compared with L-shell. Even quasars, with their non-thermal continuum, are not this hard. This will overestimate the importance of K-shell photoionization. The upper panel of Figure 9 shows this SED as νf_ν .

The photon flux ϕ_ν enters in the photoionization rate. This is the ratio $\phi_\nu \propto f_\nu/h\nu \propto \nu^{-2}$. This is shown in the lower panel. The flux of K-shell photons is about 150 times smaller than the flux of L shell photons.

Cloudy includes a command to report each shell's photoionization rate Γ_n . We need this to treat Auger electron ejection and fluorescent emission properly. That rate is shown in the following Table 1.

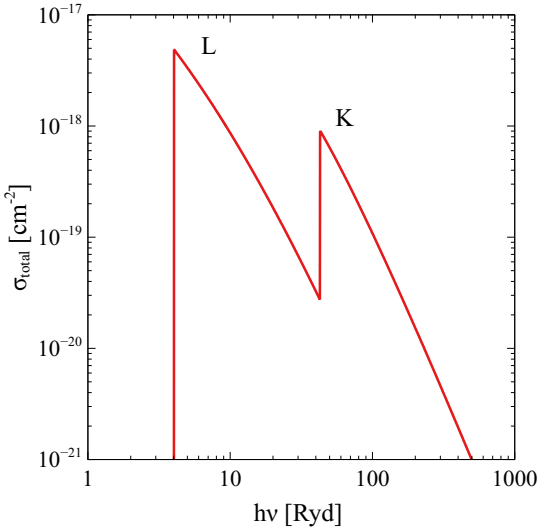


Fig. 8. The total opacity of doubly ionized oxygen is shown. The K and L shell edges are marked. The color figure can be viewed online.

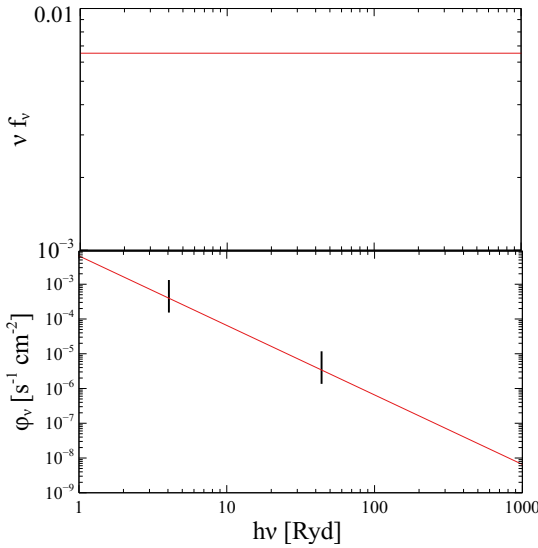


Fig. 9. The upper panel shows the SED for an $f_\nu \propto \nu^{-1}$ SED, an exceptionally hard continuum. The lower panel gives the photon flux, $\phi_\nu \propto f_\nu/h\nu \propto \nu^{-2}$. The hash marks indicate the locations of the K and L shells. The photon flux in the K shell is ≈ 2 dex smaller than the L shell. The color figure can be viewed online.

The L shell rates are about 150 times larger than the K shell rates, due to the different photon fluxes, cross-sections, and energy ranges. The implication is that the K-shell rates are negligible compared with the valence shell rates. One result is that differences in the X-ray portion of a SED will have little impact on UV - IR emission.

TABLE 1

PHOTOIONIZATION RATES PER SUBSHELL

Shell	Γ_n
$1s^2$	8.84×10^{-13}
$2s^2$	4.71×10^{-14}
$2p^2$	1.28×10^{-10}

There were several papers published in the 1970s that discussed inner shell processes at length. This physics is fully included in Cloudy. Many of those papers overstated the importance of inner shell physics on the ionization.

Although the inner shell physics has little effect on the ionization of the gas, it will be important for producing X-ray fluorescent emission lines as well as X-ray transmission spectroscopy. High-resolution X-ray observations of absorbing clouds in front of the X-ray continuum source could measure the features.

7. MISCELLANEOUS IMPROVEMENTS

The photoionization thresholds of most ions have been slightly updated as of C17.02. In this release, the entries for the radiative recombination continua on the line stack have updated wavelengths to make them consistent with the new thresholds.

The ionization potentials employed by CLOUDY have been updated. The new values are extracted from NIST and are current as of 2022-11-15. The differences between the datasets for the elements up to zinc are at most 0.5%. In addition, in preparation for future development, our ionization potential data set includes all natural elements and all their ions. That is, our list extends up to plutonium, instead of up to krypton.

The solar abundances of Lodders et al. (2009) have been added to CLOUDY as of C17.01.

To fix a bug where many blends were not predicted on the emergent line stack, the requirements for adding lines to a blend have been tightened. Blend components now have to be transmitted lines (i.e. have type 't', as indicated in the **save line labels** output) that are associated to a database transition. As a result, many blend components have been removed, mostly predictions for the recombination contribution to a given line. These predictions were based on ad hoc theories that are invalid over the entire parameter range that CLOUDY covers. The components that have been removed are still available as separate entries on the line stack.

Detailed information about the changes can be found on our wiki.¹⁶

The label for the inward component of continuum bands has been changed to “InwdBnd”. Previously that was “Inwd”. This led to ambiguities with individual Fe II lines when the big Fe II model was used.

The labels for collisional heating and cooling of the gas by grains have been renamed to “GrCH” and “GrCC”, respectively. Previously, they were both called “GrGC”.

The code now uses the 2018 CODATA adjustment for the fundamental physical constants.

8. SEDS IN CLOUDY

Support for the Khaire & Srianand (2019) synthesis models of the extragalactic background light has been added since C17.01. These SEDs cover the range from the far infrared to TeV γ -rays, with an emphasis on the extreme ultraviolet background responsible for the observed ionization of the intergalactic medium for redshifts between $0 \leq z \leq 15$.

In addition, four AGN SEDs described by Jin et al. (2012) and Jin et al. (2017) are now included, see Figure 10, as well as the SED for NGC 5548 of Dehghanian et al. (2019).

9. INFRASTRUCTURE CHANGES

9.1. Migration to C++11

The code has been ported to C++11. This version of the C++ standard delivers significant new functionality and fixes many issues with the old C++98 standard we were using until now. Adopting the new standard enables writing more versatile code. Compilers with full support for the C++11 standard have been available since April 2013 (though some vendors only finalized their support later). By now, these compilers should be widely available, and this change should not impact the ability of our users to use CLOUDY. Users now need a compiler with the following minimum requirements. For GNU g++ version 4.8.1 or later, for LLVM clang++ version 3.3 or later, for the Intel compiler version 15.0 or later, and for the Oracle Developer Studio compiler version 12.5 or later.

9.2. Executing the Code

CLOUDY now supports the `-e` flag on the command line. After this flag, the user may enter one or more CLOUDY commands separated by a semicolon. This averts the need to create an input file

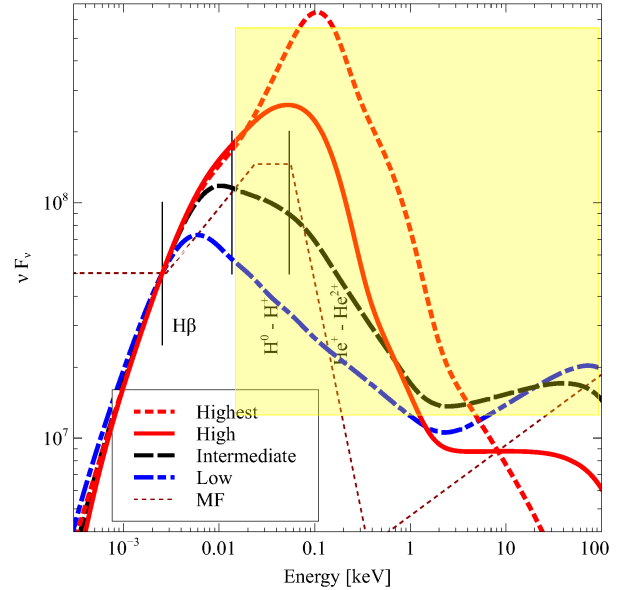


Fig. 10. This figure, from Ferland et al. (2020), compares the SEDs of Jin et al. (2012) and Jin et al. (2017) over a range of Eddington ratio. The curve marked “MF” is taken from Mathews & Ferland (1987) and obtained with the **TABLE AGN** command. The color figure can be viewed online.

for very simple (test) models. It can also be useful when calling CLOUDY from a shell script.

The executable now accepts the `-s [seed]` command line flag. This will set a fixed seed for the random number generator and is intended for debugging and testing purposes. The parameter is a 64-bit seed in hexadecimal form. If the seed is omitted, a default fixed value will be used. It is not recommended to use this flag in normal CLOUDY runs.

The `-a` flag on the command line has been removed. This flag was only used in debugging and had been deprecated for some time.

The code has been enhanced to catch floating point exceptions and segmentation faults on supported platforms (this includes all major compilers on Linux and MacOS). This makes grid runs even more resilient against errors in one of the grid models, allowing the code to finish the grid despite these errors.

If some models in a grid fail, the **save** output for that grid point may be missing. As a workaround, the code now creates a stub file for the missing output by taking the correct output from another grid point and replacing all numbers by zeros.

In previous versions, when CLOUDY aborted (e.g. due to too many convergence failures) it would try to soldier on and produce some (most likely wrong)

¹⁶<https://gitlab.nublado.org/cloudy/cloudy/-/wikis/NewC22>

output despite the failure. This is no longer done. The code now stops immediately after the abort.

Most compilers will now generate a backtrace of the call stack at the end of the output if an error occurs. This is useful for debugging purposes.

9.3. Reading and Writing Files

For several years CLOUDY allowed the user to supply a custom search path for searching data files. The development of this feature has now been finalized. The code now uses a consistent policy for finding files that it needs to read. All commands will look in the local directory first, and then in the data directory (this is the standard search path). The user can alter the search path by defining the environment variable `CLOUDY_DATA_PATH` before the code is started up. This gives the user more freedom to choose where custom data files are stored. Setting this variable will no longer affect the compilation of the code (as was the case in C17 and before). The code will always write output in the local directory. This is now enforced.

9.4. Parser Changes

We have started modifying the parser to check the script's syntax more strictly. The long-term goal is to check everything that is typed. In this release, we will start by fully checking the command name itself. Abbreviating the command is still allowed (as was already the case in previous releases) but all the typed characters will now be checked. We will enforce US spelling where relevant.

The input deck's set of allowed comment characters has been significantly reduced. Since version C17.01, it is no longer allowed to use "c" or "C" to start a comment. In the current version, only comments starting with "#" or "##" are allowed. Comments of the first type will be echoed in the main output, while comments starting with "##" will not be echoed.

The parser now supports line disambiguation. The CLOUDY line stack may contain seemingly duplicate entries with the same label and wavelength but which are actually different lines. This can create problems if you want to use such a line. One example is the H I 4.65247 μm line, which may be either the $7 \rightarrow 5$ or the $35 \rightarrow 7$ line. You can now optionally supply the lower and upper level index, or the energy of the lower level, to indicate which line you want. The **save line labels** output contains the necessary information to do this. This new syntax is supported by all commands that read line identifications. It is also supported by the subroutines *cdLine*, *cdEmis*, and *cdGetLineList*. This type

of disambiguation is not possible for all lines on the line stack.

9.5. Numerical Methods

The old random number generators have been removed from CLOUDY. These were based on the Mersenne twister algorithm and the Box-Muller method for generating random numbers with a normal (Gaussian) distribution. The new code uses a fully vectorized version of xoshiro256** (Blackman & Vigna 2021)¹⁷, while the random numbers with a normal distribution are now generated using the Ziggurat algorithm (Marsaglia & Tsang 2000). Both methods are much faster than the old ones. An additional advantage is that the new code is fully aware of parallelization in the code, meaning that parallel ranks created with MPI or fork will automatically have a different sequence of random numbers. The code now generates a random seed at the start of execution by default (when available derived from `/dev/urandom`, otherwise using the system time), unless the `-s` command line parameter described above is used.

9.6. New, Modified, and Deleted Commands

Since C17.01 the **save xspec** command has a new option **normalize**. In versions prior to C17, the spectra would always have the same normalization as the **save continuum** output. This can be inconvenient for comparing spectra in grids where the normalization of the spectra can be vastly different. When using the **normalize** keyword, all spectra will be normalized to $1 \text{ photon cm}^{-2} \text{ s}^{-1} \text{ keV}^{-1}$ at a photon energy of 1 keV. The user can alter the latter value to a different photon energy.

Since C17.02, the **save transmitted continuum** command also works in luminosity mode, and the keyword **last** is implicitly assumed to avoid useless output. The format of the **save transmitted continuum** file has changed, so files from versions C17.01 and older will no longer be accepted. Spherical dilution will now be implicitly handled when the keyword **scale** is used, and the first and second models both set a radius.

The command **database h-like keep fine structure** has been added. This allows the fine-structure components of the hydrogen-like lines to be reported on the line stack. Previous versions of the code already computed these components but did not report them. This behavior is still the default, but by including this command, the fine-structure lines will be added to the line stack.

¹⁷<http://xoshiro.di.unimi.it>.

The commands **crash segfault**, **crash abort**, **crash grid**, and **crash bounds array** have been added to emulate additional sources of errors. The **crash bounds heap** command has been removed as CLOUDY no longer uses this method of allocating memory. The **crash undefined** commands have been reorganized and the only option left (without any additional keywords) is to test access to an undefined variable on the stack (this used to be called **crash undefined stack | auto**).

The **set assert abort** command has been removed. Its effect was identical to the **-a** command line flag, which was only used for debugging the code. The **stop nTotalIoniz** command has been removed. This was a debugging tool that was very rarely used. The **drive** family of commands have been removed. These were designed to test certain aspects of the code interactively. They have not been used in a long time and are obsolete. The **state** command has been removed. This was an unfinished experimental feature to save or restore the state of the code. This project has now been abandoned as it was too difficult to do. The **plot** family of commands has been removed (as was already announced in HAZY). This was obsolete code for producing ASCII plots on line printers.

The option to set the seed for the random number generator has been removed from the **database H2 noise** and **database H-like | He-like error generation** commands. Using a random seed is now the default, so the user is no longer needed to set the seed.

The **table SED** command now accepts the **Flambda** keyword in the SED data file. Fluxes in F_ν or νF_ν units were already accepted, now F_λ units can also be used.

The upper limit to the number of lines that can be supplied to the **print line sum** and **save lines emissivity** commands has been removed.

The command **set blend** has been added, allowing the user to define custom line blends. This command allowed us to move most of the blends that used to be hardwired into the code (e.g., Bldn 1909) to a new init file called **blends.ini** that is part of the data directory. This file is parsed automatically when starting up CLOUDY, unless the **no blends** command is included in the script.

The **abundances** command has been modified. It is now mandatory to include an element symbol in front of the abundance, which will determine what element the abundance belongs to. This makes the command much safer. It also allows the user to put the elements in arbitrary order and removes the need

to complete the list of abundances. The **elements read** command has been removed as it is no longer needed.

The **database He-like FSM** command has been removed. It was not working correctly, and moreover, Bauman et al. (2005) found that as a result of the principle of spectroscopic stability, it had very little impact on the predictions for the He I spectrum. The situation is different, though, for highly charged ions, e.g. Fe XXV. For such ions, the individual fine-structure components can be spectroscopically resolved and treating fine-structure mixing would be warranted. Implementing this will be postponed to a future release.

9.7. Storing SED Grids

The SED grids supported by CLOUDY no longer need to be compiled into binary form. The code now directly reads the ASCII files to obtain the necessary information. Compiling the ASCII files is still supported, but now produces a completely different type of file that contains indices into the ASCII file. This step is optional but is strongly recommended for large grids to speed up the code. With this setup, recompiling stellar atmosphere grids is no longer necessary when the frequency mesh is changed. Compiling SEDs in an external format (such as Starburst99 or the Rauch stellar atmosphere grids) is still mandatory to obtain the ASCII files.

10. FUTURE DIRECTIONS

Work is under way to extend and improve CLOUDY. Some of these features will be available, at least in part, by the time of the next release, while others may require longer to come to fruition. Some of these directions were already discussed by van Hoof et al. (2020).

As explained above, the X-ray capabilities of CLOUDY have been extended substantially. Yet, more work remains to be done. We are currently working on resolving the doublets of Lyman-like emission lines ($np \rightarrow 1s$ transitions) in hydrogenic ions (Gunasekera, in preparation). This feature should be available in the next major release. In addition, we plan to extend CLOUDY to include the results of experiments on inner-shell ionization. In the longer run, we should update the charge-exchange data of the code with modern calculations, e.g., with the Kronos database¹⁸ (e.g., Mullen et al. 2016; Cumbee et al. 2016, 2018; Lyons et al. 2017).

Over the last one or two decades, astronomy has entered its high-precision era. So must CLOUDY.

¹⁸<https://www.physast.uga.edu/research/stancil-group/atomic-molecular-databases/kronos>

Given that much of what we know about the chemical composition and kinematics of celestial sources comes from spectroscopy, it is of paramount importance to improve the atomic data the code employs to make quantitative predictions for, and to interpret, observations. A program is underway (PI: Chatzikos) to produce high-quality atomic data that combine laboratory-grade wavelengths (i.e., energies) with accurate transition probabilities and collision strengths. The new models will be added to our Stout database.

Other aspects of CLOUDY that are under active development include time-dependent calculations and the radiative transfer module of the code. We aim to publicly release these updates in the next one or two releases.

MC acknowledges support from NSF (1910687), NASA (19-ATP19-0188, 22-ADAP22-0139), and STScI (HST-AR-14556.001-A). GJF acknowledges support by NSF (1816537, 1910687), NASA (ATP 17-ATP17-0141, 19-ATP19-0188), and STScI (HST-AR- 15018 and HST-GO-16196.003-A). SB acknowledges support from PRIN MUR 2017 “Black hole winds and the baryon life cycle of galaxies: the stone-guest at the galaxy evolution supper” and from the European Union Horizon 2020 Research and Innovation Framework Programme under grant agreement AHEAD2020 n.871158. GS acknowledges WOS-A grant from the Department of Science and Technology (SR/WOS-A/PM-2/2021). GS thanks Ziwei Zhang for providing the vib-rotational data of SiS.

REFERENCES

- Amato, R., Grinberg, V., Hell, N., et al. 2021, *A&A*, 648, 105, <https://doi.org/10.1051/0004-6361/202039125>
- Anusuri, B. 2019, *Heliyon*, 5, e01647, <https://doi.org/10.1016/j.heliyon.2019.e01647>
- Badnell, N. R. & Ballance, C. P. 2014, *ApJ*, 785, 99, <https://doi.org/10.1088/0004-637X/785/2/99>
- Badnell, N. R., Guzmán, F., Brodie, S., et al. 2021, *MNRAS*, 507, 2922, <https://doi.org/10.1093/mnras/stab2266>
- Baker, J. G. & Menzel, D. H. 1938, *ApJ*, 88, 52, <https://doi.org/10.1086/143959>
- Baldwin, J. A., Ferland, G. J., Korista, K. T., Hamann, F., & LaCluzé, A. 2004, *ApJ*, 615, 610, <https://doi.org/10.1086/424683>
- Bauman, R. P., Porter, R. L., Ferland, G. J., & MacAdam, K. B. 2005, *ApJ*, 628, 541, <https://doi.org/10.1086/430665>
- Bautista, M. A., Fivet, V., Ballance, C., et al. 2015, *ApJ*, 808, 174, <https://doi.org/10.1088/0004-637X/808/2/174>
- Blackman, D. & Vigna, S. 2021, *ACM Trans. Math. Softw.*, 47, <https://doi.org/10.1145/3460772>
- Bruhweiler, F. & Verner, E. 2008, *ApJ*, 675, 83, <https://doi.org/10.1086/525557>
- Bundy, K., Bershady, M. A., Law, D. R., et al. 2015, *ApJ*, 798, 7, <https://doi.org/10.1088/0004-637X/798/1/7>
- Camilloni, F., Bianchi, S., Amato, R., Ferland, G., & Grinberg, V. 2021, *RNAAS*, 5, 149, <https://doi.org/10.3847/2515-5172/ac0cff>
- Chakraborty, P., Ferland, G. J., Bianchi, S., & Chatzikos, M. 2020a, *RNAAS*, 4, 184, <https://doi.org/10.3847/2515-5172/abc1dd>
- Chakraborty, P., Ferland, G. J., Chatzikos, M., et al. 2022, *ApJ*, 935, 70, <https://doi.org/10.3847/1538-4357/ac7eb9>
- Chakraborty, P., Ferland, G. J., Chatzikos, M., Guzmán, F., & Su, Y. 2020b, *ApJ*, 901, 68, <https://doi.org/10.3847/1538-4357/abaaab>
- _____. 2020c, *ApJ*, 901, 69, <https://doi.org/10.3847/1538-4357/abaaac>
- _____. 2021, *ApJ*, 912, 26, <https://doi.org/10.3847/1538-4357/abed4a>
- Chamberlain, J. W. 1953, *ApJ*, 117, 399, <https://doi.org/10.1086/145705>
- Cumbee, R. S., Liu, L., Lyons, D., et al. 2016, *MNRAS*, 458, 3554, <https://doi.org/10.1093/mnras/stw527>
- Cumbee, R. S., Mullen, P. D., Lyons, D., et al. 2018, *ApJ*, 852, 7, <https://doi.org/10.3847/1538-4357/aa99d8>
- Dehghanian, M., Ferland, G. J., Kriss, G. A., et al. 2019, *ApJ*, 877, 119, <https://doi.org/10.3847/1538-4357/ab1b48>
- Doddipatla, S., He, C., Goettl, S. J., et al. 2021, *SciA*, 7, <https://doi.org/10.1126/sciadv.abg7003>
- Draine, B. T. 2003, *ApJ*, 598, 1026, <https://doi.org/10.1086/379123>
- Ferland, G. J. 1999, *PASP*, 111, 1524, <https://doi.org/10.1086/316466>
- Ferland, G. J., Chatzikos, M., Guzmán, F., et al. 2017, *RMxAA*, 53, 385, <https://doi.org/10.48550/arXiv.1705.10877>
- Ferland, G. J., Done, C., Jin, C., Landt, H., & Ward, M. J. 2020, *MNRAS*, 494, 5917, <https://doi.org/10.1093/mnras/staa1207>
- Ferland, G. J., Korista, K. T., Verner, D. A., et al. 1998, *PASP*, 110, 761, <https://doi.org/10.1086/316190>
- Ferland, G. J., Porter, R. L., van Hoof, P. A. M., et al. 2013, *RMxAA*, 49, 137, <https://doi.org/10.48550/arXiv.1302.4485>
- Fernández-Menchero, L., Del Zanna, G., & Badnell, N. R. 2014, *A&A*, 572, 115, <https://doi.org/10.1051/0004-6361/201424849>
- Fujimoto, T. 1978, *Semi-Empirical Cross Section and Rate Coefficients for Excitation and Ionization by*

- Electron Collision and Photoionization of Helium. Institute of Plasma Physics Report, Japan, IIP Jam-8, Nagoya University
- Gunasekera, C. M., Chatzikos, M., & Ferland, G. J. 2022a, *Astro*, 1, 255, <https://doi.org/10.3390/astronomy1030015>
- Gunasekera, C. M., Ji, X., Chatzikos, M., Yan, R., & Ferland, G. 2022b, *MNRAS*, 512, 2310, <https://doi.org/10.1093/mnras/stac022>
- _____. 2023, *MNRAS*, 520, 4345, <https://doi.org/10.1093/mnras/stad322/mnras/stad322>
- Guzmán, F., Badnell, N. R., Chatzikos, M., van Hoof, P. A. M., Williams, R. J. R., & Ferland, G. J. 2017a, *MNRAS*, 467, 3944, <https://doi.org/10.1093/mnras/stx269>
- Guzmán, F., Badnell, N. R., Williams, R. J. R., van Hoof, P. A. M., Chatzikos, M., & Ferland, G. J. 2016, *MNRAS*, 459, 3498, <https://doi.org/10.1093/mnras/stw893>
- _____. 2017b, *MNRAS*, 464, 312, <https://doi.org/10.1093/mnras/stw2304>
- Guzmán, F., Chatzikos, M., van Hoof, P. A. M., Balser, D. S., Dehghanian, M., Badnell, N. R., & Ferland, G. J. 2019, *MNRAS*, 486, 1003, <https://doi.org/10.1093/mnras/stz857>
- Hell, N., Brown, G. V., Wilms, J., et al. 2016, *ApJ*, 830, 26, <https://doi.org/10.3847/0004-6347X/830/1/26>
- Jenkins, E. B. 2009, *ApJ*, 700, 1299, <https://doi.org/10.1088/0004-637X/700/2/1299>
- Jin, C., Done, C., Ward, M., & Gardner, E. 2017, *MNRAS*, 471, 706, <https://doi.org/10.1093/mnras/stx1634>
- Jin, C., Ward, M., & Done, C. 2012, *MNRAS*, 425, 907, <https://doi.org/10.1111/j.1365-2966.2012.21272.x>
- Kaastra, J. S. & Mewe, R. 1993, *A&AS*, 97, 443
- Khaire, V. & Srikanand, R. 2019, *MNRAS*, 484, 4174, <https://doi.org/10.1093/mnras/stz174>
- Komasa, J., Piszczatowski, K., Lach, G., et al. 2011, *Journal of Chemical Theory and Computation*, 7, 3105, *J. Chem. Theory Comput.*, 7, 10, <https://doi.org/10.1021/ct200438t>
- Kramida, A., Ralchenko, Y., Nave, G., & Reader, J. 2018, APS Division of Atomic and Molecular Physics Meeting, abstract id.M01.004
- Laha, S., Tyndall, N. B., Keenan, F. P., et al. 2017, *ApJ*, 841, 3, <https://doi.org/10.3847/1538-4357/aa7071>
- Lebedev, V. S. & Beigman, I. L. 1998, *Physics of highly excited atoms and ions* (Berlin, Heidelberg: Springer)
- Liang, G. Y. & Badnell, N. R. 2011, *A&A*, 528, 69, <https://doi.org/10.1051/0004-6361/201016417>
- Liang, G. Y., Whiteford, A. D., & Badnell, N. R. 2009, *A&A*, 500, 1263, <https://doi.org/10.1051/0004-6361/200911866>
- Liedahl, D. A. 2005, *AIPC* 774, X-RAY DIAGNOSTICS OF ASTROPHYSICAL PLASMAS: Theory, Experiment, and Observation, 99, <https://doi.org/10.1063/1.1960918>
- Lique, F. 2015, *MNRAS*, 453, 810, <https://doi.org/10.1093/mnras/stv1683>
- Lodders, K., Palme, H., & Gail, H.-P. 2009, *LanB*, 4, 712, (Berlin Heidelberg: Springer), https://doi.org/10.1007/978-3-540-88055-4_34
- Lykins, M. L., Ferland, G. J., Kisieliuss, R., et al. 2015, *ApJ*, 807, 118, <https://doi.org/10.1088/0004-637X/807/2/118>
- Lyons, D., Cumbee, R. S., & Stancil, P. C. 2017, *ApJS*, 232, 27, <https://doi.org/10.3847/1538-4365/aa8d16>
- Marsaglia, G. & Tsang, W. W. 2000, *Journal of Statistical Software*, 5, 1, <https://doi.org/10.18637/jss.v005.i08>
- Mathews, W. G. & Ferland, G. J. 1987, *ApJ*, 323, 456, <https://doi.org/10.1086/165843>
- Matt, G., Brandt, W. N., & Fabian, A. C. 1996, *MNRAS*, 280, 823, <https://doi.org/10.1093/mnras/280.3.823>
- Menzel, D. H. 1937, *ApJ*, 85, 330, <https://doi.org/10.1086/143827>
- Mullen, P. D., Cumbee, R. S., Lyons, D., & Stancil, P. C. 2016, *ApJS*, 224, 31, <https://doi.org/10.3847/0067-0049/224/2/31>
- Netzer, H. 2020, *MNRAS*, 494, 1611, <https://doi.org/10.1093/mnras/staa767>
- Osterbrock, D. E. & Ferland, G. J. 2006, *Astrophysics of gaseous nebulae and active galactic nuclei*, 2nd. ed. D. E. Osterbrock and G. J. Ferland (Sausalito, CA: University Science Books)
- Peimbert, M., Peimbert, A., & Delgado-Inglada, G. 2017, *PASP*, 129, 082001, <https://doi.org/10.1088/1538-3873/aa72c3>
- Pengelly, R. M. & Seaton, M. J. 1964, *MNRAS*, 127, 165, <https://doi.org/10.1093/mnras/127.2.165>
- Priestley, F. D., Barlow, M. J., & Viti, S. 2017, *MNRAS*, 472, 4444, <https://doi.org/10.1093/mnras/stx2327>
- Röllig, M. 2011, *A&A*, 530, 9, <https://doi.org/10.1051/0004-6361/201014743>
- Ross, R. R., Weaver, R., & McCray, R. 1978, *ApJ*, 219, 292, <https://doi.org/10.1086/155776>
- Roueff, E., Alekseyev, A. B., & Le Bourlot, J. 2014, *A&A*, 566, 30, <https://doi.org/10.1051/0004-6361/201423652>
- Sarkar, A., Ferland, G. J., Chatzikos, M., et al. 2021, *ApJ*, 907, 12, <https://doi.org/10.3847/1538-4357/abcaa6>
- Schilke, P., Neufeld, D. A., Müller, H. S. P., et al. 2014, *A&A*, 566, 29, <https://doi.org/10.1051/0004-6361/201423727>
- Shaw, G., Ferland, G., & Chatzikos, M. 2023a, *RNAAS*, 7, 45, <https://doi.org/10.3847/2515-5172/acclaa>
- _____. 2023b, *RNASS*, 7, 153, <https://doi.org/10.3847/2515-5172/ace9b5>

- Shaw, G. & Ferland, G. J. 2021, *ApJ*, 908, 138, <https://doi.org/10.3847/1538-4357/abdab2>
- Shaw, G., Ferland, G. J., Abel, N. P., Stancil, P. C., & van Hoof, P. A. M. 2005, *ApJ*, 624, 794, <https://doi.org/10.1086/429215>
- Shaw, G., Ferland, G. J., & Chatzikos, M. 2022, *ApJ*, 934, 53, <https://doi.org/10.3847/1538-4357/ac7789>
- Shaw, G., Ferland, G. J., & Ploeckinger, S. 2020, *RNAAS*, 4, 78, <https://doi.org/10.3847/2515-5172/ab97ae>
- Si, R., Li, S., Wang, K., et al. 2017, *A&A*, 600, 85, <https://doi.org/10.1051/0004-6361/201630027>
- Smyth, R. T., Ramsbottom, C. A., Keenan, F. P., Ferland, G. J., & Ballance, C. P. 2019, *MNRAS*, 483, 654, <https://doi.org/10.1093/mnras/sty3198>
- Tayal, S. S. & Zatsarinny, O. 2018, *PHRvA*, 98, 012706, <https://doi.org/10.1103/PhysRevA.98.012706>
- Temple, M. J., Matthews, J. H., Hewett, P. C., et al. 2023, *MNRAS*, 523, 646, <https://doi.org/10.1093/mnras/stad1448>
- Toboła, R., Lique, F., Klos, J., & Chalasiński, G. 2008, 2008, *JPhB*, 41, 155702, <https://doi.org/10.1088/0953-4075/41/15/155702>
- van der Tak, F. F. S., Lique, F., Faure, A., Black, J. H., & van Dishoeck, E. F. 2020, *Atoms*, 8, 15, <https://doi.org/10.3390/atoms8020015>
- van Hoof, P. A. M., Van de Steene, G. C., Guzmán, F., et al. 2020, *CoSka*, 50, 32, <https://doi.org/10.31577/caosp.2020.50.1.32>
- van Regemorter, H. 1962, *ApJ*, 136, 906, <https://doi.org/10.1086/147445>
- Verner, D. A., Ferland, G. J., Korista, K. T., & Yakovlev, D. G. 1996, *ApJ*, 465, 487, <https://doi.org/10.1086/177435>
- Verner, E. M., Verner, D. A., Baldwin, J. A., Ferland, G. J., & Martin, P. G. 2000, *ApJ*, 543, 831, <https://doi.org/10.1086/317159>
- Verner, E. M., Verner, D. A., Korista, K. T., Ferguson, J. W., Hamann, F., & Ferland, G. J. 1999, *ApJS*, 120, 101, <https://doi.org/10.1086/313171>
- Vestergaard, M. & Wilkes, B. J. 2001, *ApJS*, 134, 1, <https://doi.org/10.1086/320357>
- Vincent, L. F. M., Spielfiedel, A., & Lique, F. 2007, *A&A*, 472, 1037, <https://doi.org/10.1051/0004-6361:20077869>
- Vriens, L. & Smeets, A. H. M. 1980, *Phys. Rev. A*, 22, 940, <https://doi.org/10.1103/PhysRevA.22.940>
- Vrinceanu, D. & Flannery, M. R. 2001, *Phys. Rev. A*, 63, 032701, <https://doi.org/10.1103/PhysRevA.63.032701>
- Vrinceanu, D., Onofrio, R., Oonk, J. B. R., Salas, P., & Sadeghpour, H. R. 2019, *ApJ*, 879, 115, <https://doi.org/10.3847/1538-4357/ab218c>
- Vrinceanu, D., Onofrio, R., & Sadeghpour, H. R. 2012, *ApJ*, 747, 56, <https://doi.org/10.1088/0004-637X/747/1/56>
- . 2017, *MNRAS*, 471, 3051, <https://doi.org/10.1093/mnras/stx1783>
- Wang, T., Ferland, G. J., Yang, C., Wang, H., & Zhang, S. 2016, *ApJ*, 824, 106, <https://doi.org/10.3847/0004-637X/824/2/106>
- Willacy, K. & Cherchneff, I. 1998, *A&A*, 330, 676
- Yan, R., Bundy, K., Law, D. R., et al. 2016, *AJ*, 152, 197, <https://doi.org/10.3847/0004-6256/152/6/197>
- Zanchet, A., Roncero, O., Agúndez, M., & Cernicharo, J. 2018, *ApJ*, 862, 38, <https://doi.org/10.3847/1538-4357/aaccff>
- Zhang, H. 1996, *A&AS*, 119, 523
- Zhang, H. & Sampson, D. H. 1987, *ApJS*, 63, 487, <https://doi.org/10.1086/191171>
- S. Bianchi: Dipartimento di Matematica e Fisica, Università degli Studi Roma Tre, via della Vasca Navale 84, 00146 Roma, Italy (stefano.bianchi@uniroma3.it).
- F. Camilloni: Max-Planck-Institut für extraterrestrische Physik, Giessenbachstraße, 85748 Garching, Germany (fcam@mpe.mpg.de).
- P. Chakraborty: Center for Astrophysics | Harvard & Smithsonian, Cambridge, MA (priyanka.chakraborty@cfa.harvard.edu).
- M. Chatzikos: Physics & Astronomy, University of Kentucky, Lexington KY 40506 (mchatzikos@uky.edu).
- G. Ferland: Physics & Astronomy, University of Kentucky, Lexington KY 40506 (gary@uky.edu).
- C. Gunasekera: Physics & Astronomy, University of Kentucky, Lexington KY 40506 (cmgunasekera@uky.edu).
- F. Guzmán: Physics and Astronomy, University of North Georgia, Dahlonega GA 30597 (francisco.guzmanfulgencio@ung.edu).
- J. Milby: Arts & Sciences Hive, University of Kentucky, Lexington KY 40506 (jon@uky.edu).
- A. Sarkar: Kavli Institute for Astrophysics and Space Research, Massachusetts Institute of Technology, 70 Vassar St, Cambridge, MA 02139, USA (arnabsar@mit.edu)
- G. Shaw: Department of Astronomy and Astrophysics, Tata Institute of Fundamental Research, Mumbai 400005, India (gargishaw@gmail.com).
- P. A. M. van Hoof: Royal Observatory of Belgium, Ringlaan 3, 1180 Brussels, Belgium (p.vanhoof@oma.be).